Science and Technology Journal Vol. 12 Issue: 2 June 2024 ISSN: 2321-3388

Pure CoS and Different Concentrations of Fe/Nd Co-Doped CoS Nanoparticles: Photoluminescence and Photocatalytic Studies

N. Mohondas Singh[1*], Daphilabianghun Nonglang[2], Fidelia Lalrindiki[3], and Lallianmawii[4]
[1,2,3,4]Department of Chemistry, School of Physical Sciences, Mizoram University, Aizawl-796004, India
*E-Mail: nmdas08@rediffmail.com
*Corresponding Author

Abstract—This research utilized the co-precipitation method to produce pure CoS, and Fe/Nd co-doped CoS nanoparticle with different concentrations at room temperature. The samples were characterized using UV-visible spectroscopy, FT-IR, SEM, and XRD. XRD pattern showed a cubic structure, and the Debye-Scherrer technique revealed an average particle size of 8 nm and 13 nm for 3 at.% and 5 at.% of Fe/Nd co-doped CoS. FT-IR spectroscopy identified the functional groups present and chemical bonding and the adsorption of H_2O molecules in the samples. In the prepared samples, SEM investigations revealed aggregation and the emergence of irregular forms. The excitation spectra set at 300-500 nm range with λ_{em} of 300 nm detected two broad peaks at 350 and 400 nm and a sharp peak at 470 nm. On the other hand, the emission spectrum recorded in the 400-650 nm range with λ_{ex} of 400 nm showed broad emission peaks at 420 nm, 450 nm, and 480 nm. Tauc's plot revealed that the optical bad-gap of pure and co-doped CoS nanoparticles ranged from 3.19 eV to 3.81 eV, suitable for photocatalytic activity. The testing revealed that the photocatalytic degradation of methyl red dye proved to be significantly more efficient in alkaline mediums, demonstrating clear pH dependence. Furthermore, the kinetic study for the degradation of the samples yielded R^2 values of 0.976, 0.996, and 0.991, indicating that the process followed first-order kinetics.

Keywords: Cobalt Sulphide, co-doped, XRD, photocatalytic, photoluminescence, Kinetic study.

INTRODUCTION

The method of photochemical conversion and solar energy storage using photocatalytic technology is efficient (Xu *et al.* 2020). Investigating new photocatalyst materials and their reaction processes has been emphasised over the past 20 years (Rehman *et al*., 2020). Numerous papers have studied a variety of photocatalysts, including metal-free (Mullins *et al*. 2020), metal oxides (Julkapli *et al.* 2020), metal sulphides (Wang *et al.* 2021), metal phosphides (Zhan *et al.* 2018), and metal selenides (Niasari *et al.* 2021) closely. Nevertheless, most single-component photocatalysts have demonstrated unexceptional photocatalytic performance because of the photogenerated charge carrier's quick recombination, insufficient active site, and restricted spectrum absorption.

Due to low availability, abundant resources, strong stability, and catalytic solid action, transition metal cocatalysts have recently attracted much attention in photocatalysis. Due to its ample catalytic sites, noble-metal-free cobalt sulphide (Co_xS_y) has received the most attention for replacing the noble metal cocatalyst (Jin *et al.* 2021). The CoS/Ag_2WO_4 photocatalyst was created using a simple chemical precipitation approach reported by Kokilavani *et al.*, and the composites exhibit outstanding photocatalytic degradation

 https://doi.org/10.22232/stj.2024.12.02.03

and antibacterial activity (Khan *et al.* 2021). Cobalt sulphides with various phase forms and morphologies were produced using various methods, including hydrothermal/solvothermal synthesis, spray pyrolysis, thermal breakdown, high-temperature solid phase processes, and cobalt oxide sulfuration. The preparation method significantly impacts the powder's characteristics, including particle dimensions, form, surface area, degree of crystallinity, and crystal structure, significantly impacting the material's catalytic performance.

However, the chemical co-precipitation method was employed in this work as it is a suitable approach for manufacturing large quantities of target material at a reasonable cost in light of large-scale production. The photocatalytic activity of the prepared sample was evaluated successfully in this research using an organic dye of methyl red. The co-doped and doped samples have several effects on the pure sample of CoS, which has been reported using the photoluminescence activity in this work

EXPERIMENTAL SECTION

Sample Preparation

For a pure CoS, a stoichiometric amount of $CoCl_2.6H_2O$ (1 mol) and NaS (1 mol) was taken, and solutions were made using distilled water separately. NaS solution was added to the cobalt solution drop by drop until the black precipitate appeared. It was stirred in for 1 hour, then heat was given at 70°C and kept overnight. For various atomic percentages (at.%) of dopants Fe and Nd, different percentage amounts of $FeCl_3$ and $NdCl_3$ were added to the Cobalt solution, following the same procedure. The $FeCl_3$ and $NdCl_3$ solutions were prepared with specific concentrations to achieve the desired doping levels. The precipitate was then dried in a hot air oven for 12 hours at 70°C to dry it. It was then washed four times with distilled water and finally with acetone.

Characterization of the Sample

The UV-visible absorbance spectrum and degradation studies of the sample were obtained using the UV-visible spectrophotometer EVOLUTION 220. The prepared sample was sent to FT-IR Spectroscopy (SHIMADZU CORP - 00703) to determine its absorption band. Utilising powder X-ray diffraction (XRD-BRUNKER AXS, D8 FOCUS-Powder) investigation, the phase and chemical composition of the CoS doped Fe and Nd nanoparticles were ascertained. The photoluminescence property of the sample was evaluated using the Fluorescence Spectrophotometer (F-7000). The morphology and particle size of the samples were analysed using SEM (JOEL-JSM-6390LV).

RESULTS AND DISCUSSION

XRD Study

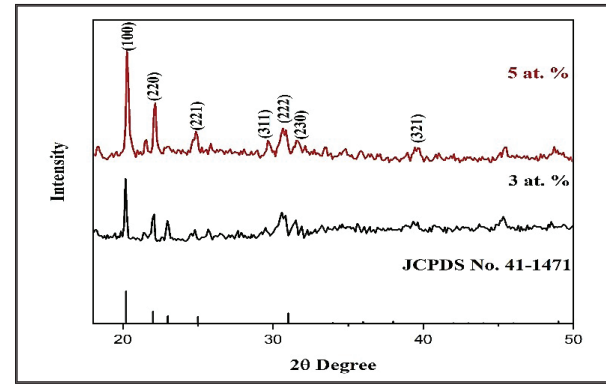

Fig. 1: Powder XRD Pattern for Fe/Nd Co-doped CoS Nanoparticles with JCPDS 41-1471 as Standard for CoS.

The X-ray diffraction (XRD) pattern of the CoS nanoparticles co-doped with 5 and 3 at.% of Fe and Nd is shown in Fig. 1. The observed peaks in the spectra show a cubic structure according to JCPDS card no. 41-1471 (Gao *et al.* 2017). The indexed diffraction peaks are assigned to (100), (220), (221), (311), (222), (230) and (321). The peaks do not show a noticeable shift after increasing Fe/Nd doping concentration, and no new phases are connected to Fe or Nd. This implies that both components have been successfully doped into the CoS structure. The average crystalline size is 3 at.% and 5 at.% Fe/Nd co-doped CoS nanoparticles were calculated using the Debye-Scherrer relation (Aghamaliyev *et al.* 2018).

$$D = 0.9\lambda / \beta \cos\theta$$

where β is the full width at half maximum (FWHM) of the peaks at diffracting angle θ, D is the crystallite diameter, and λ is the X-ray photon wavelength. The average particle size calculated is found to be 8 and 13 nm.

FTIR and Sem Study

The FTIR spectra of pure CoS and (1, 3, 5, 7, 9 and 11 at.%) Fe/Nd co-doped CoS are shown in Fig. 2. As seen in the figure, pure and doped CoS samples show similar absorption peaks at 3307, 1628, 1419, 1081, 769 and 598 cm^{-1}. The broad absorption peak at about 3307 cm^{-1} corresponds to the O-H stretching, and 1628 cm^{-1} corresponds to the O-H bending vibrations of H_2O.

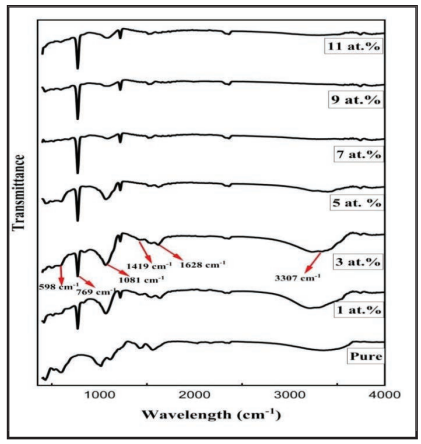

Fig. 2: FTIR Spectrum of Pure CoS and (1, 3, 5, 7, 9 and 11 at.%) Fe/Nd Co-doped CoS Nanoparticle.

The weak peak at 1419 cm^{-1} and 1081 cm^{-1} is assigned to the C-O-H deformation vibration and C-O stretching or bending vibration of sulfonated groups. In addition, the intense peak located at 769 cm^{-1} is a typical peak for the polysulfide bond group and the stretching vibration modes of Co-S. Finally, the absorption peak at 598 cm^{-1} is assigned to the stretching vibration between Co and S (Hosseinpour *et al*. 2018). As a consequence, as shown by the data above, no other phases associated with dopants were found, demonstrating the incredible purity of the samples.

Scanning Elelctron Microscopy (SEM)

Fig. 3a and b are the SEM images of the synthesized (3 and 5 at.%) Fe/Nd co-doped CoS. Small particles of various sizes in agglomerated forms were observed in both the images. The electron micrograph (Fig. 3c & d) is used to determine the average particle size, which is found to be 73.16 nm for 3 at.% and 50.18 nm for 5 at.% Fe/Nd co-doped CoS nanoparticles.

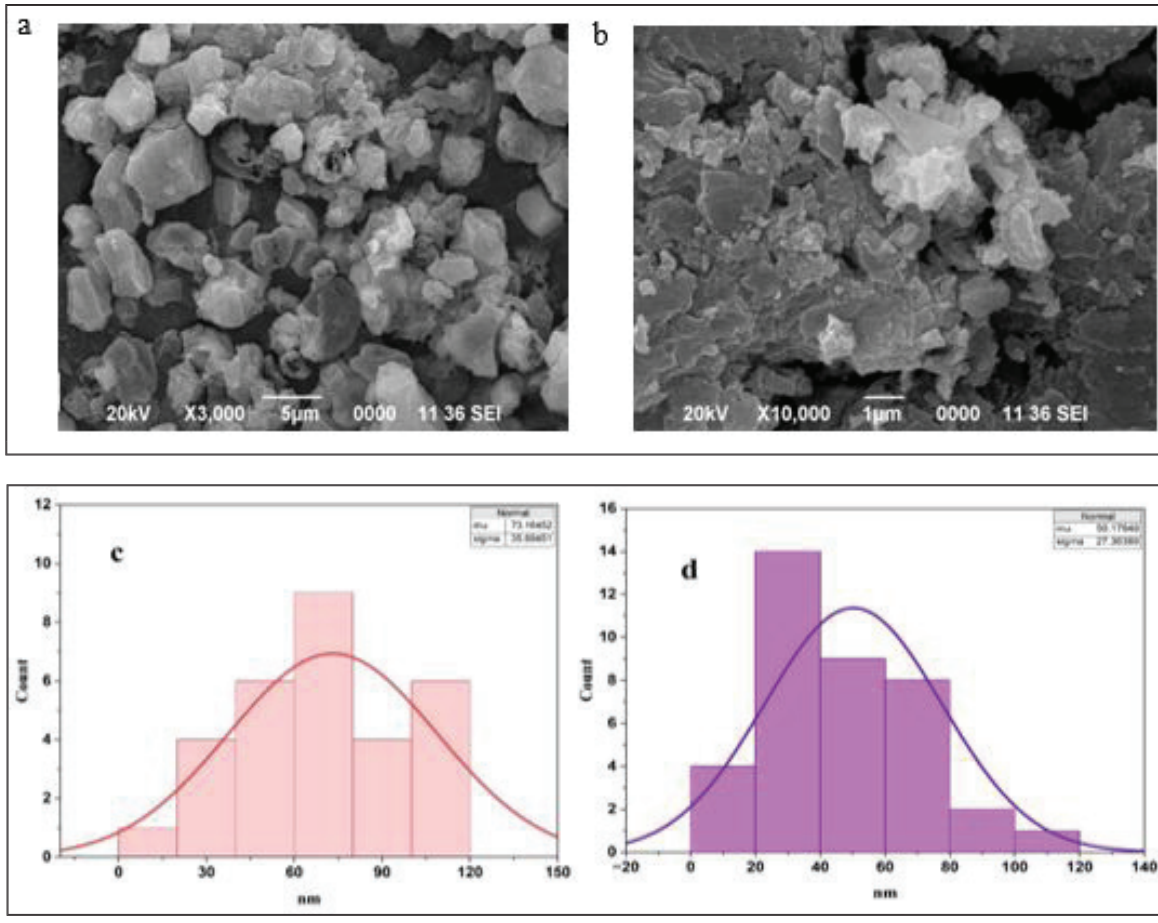

Fig. 3: (a, b) SEM Images and (c, d) Size Distribution Graphs for Average Size of (3 and 5 at.%) Fe/Nd Co-doped CoS Nanoparticles.

Photoluminescence Study

The photoluminescence studies of pure and (1, 3, 5, 7, 9 and 11 at.%) Fe/Nd co-doped CoS nanoparticles were studied for electron emission and excitation at room temperature. The excitation spectrum is observed in the 300-500 nm range at an emission wavelength of 300 nm. It displays two broad peaks in Fig. 4(a) at 350 nm and 400 nm and a strong peak at 470 nm, which agrees with the literature (Hosseinpour *et al.* 2018). The blue and violet emission peaks at 400 and 470 nm may be due to Co vacancy and S interstitial-related defects.

In Fig. 4(b), the emission spectrum is configured in the 400-650 nm range with a λ_{ex} of 400 nm. Prominent violet emission peaks at 420 nm and 450 nm are consistently observed across all the samples, accompanied by a faint blue emission peak at 480 nm.

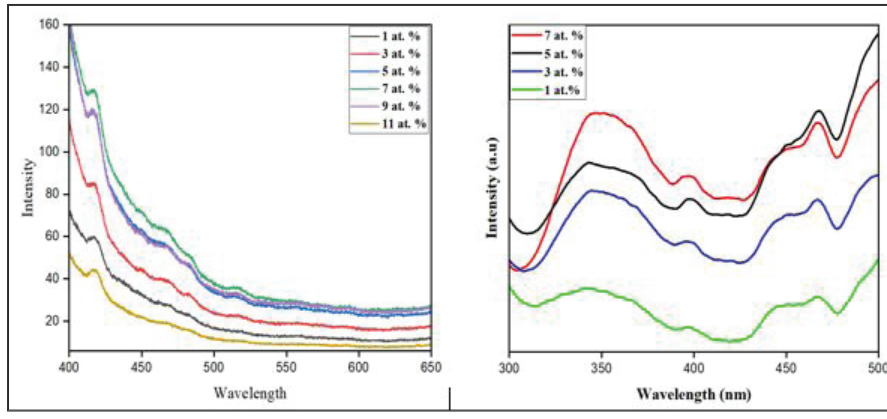

Fig. 4: (a) Photoluminescence of Pure and Different Percentages of (1, 3, 5, 7, 9 and 11 at.%) Fe/Nd Co-doped CoS Nanoparticles Using an Emission Wavelength of 300 nm and (b) Photoluminescence of Pure and Different Percentages of (1, 3, 5 and 7 at.%) Fe/Nd Co-doped CoS Nanoparticles using an Excitation Wavelength of 400nm.

CIE Analysis

Fig. 5 illustrates the CIE chromaticity diagram for the samples in their prepared state for pure and (3 and 5 at.%) Fe/Nd co-doped CoS calculated using the emission spectrum data observed when stimulated at 470 nm. For the samples that were created, the determined colour coordinates (x, y) are (0.236, 0.389), (0.236, 0.322), and (0.313, 0.204), respectively. This graphic shows the bluish-green region in all of the samples, and the inset shows the colour of the emission observed following UV light excitation at 470 nm (Singh *et al*. 2022).

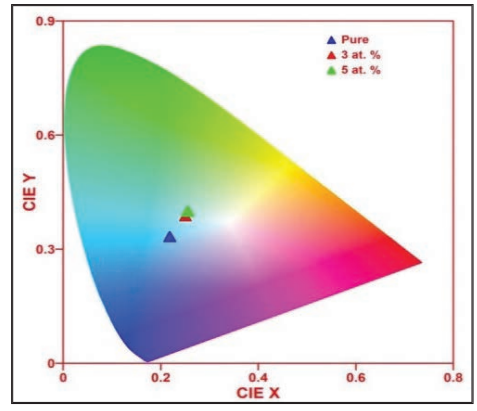

Fig. 5: CIE Chromaticity Diagram for as Prepared Pure CoS, 3 at.% Fe/Nd Co-doped CoS and 5 at.% Fe/Nd Co-doped CoS Nanaoparticles.

Lifetime Study

The decay curves were measured with the excitation fixed at 470 nm for each concentration. The curves of the measured deterioration are shown in Fig. 6. All reported decay curves fit well with the biexponential equation. The samples' fit (R^2) qualities for the concentrations above are 0.9152, 0.9573, and 0.9636, respectively, and their estimated average lifetimes are 1.21, 1.36, and 1.73 ms, respectively (Singh *et al*. 2018).

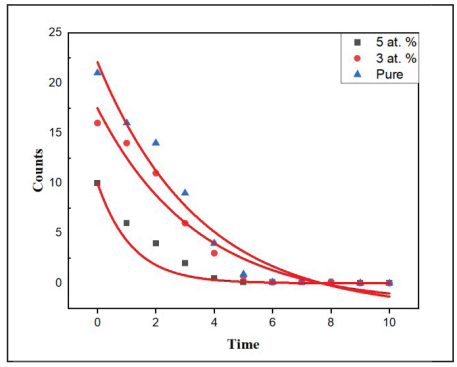

Fig. 6: Decay Curves for as Prepared Pure CoS, 3 at.%, 5 at. % Fe/Nd Co-doped CoS Samples.

Optical Properties Analysis

The optical properties after Fe and Nd have been successfully incorporated into CoS (1, 3, 5, 7, 9 and 11 at.%) were investigated using a UV-visible spectrometer as shown in Fig. 7 and were observed in the wavelength range of 200-400nm. According to the literature, the absorption peak for CoS was speculated to be around 210 nm (Sundararajan *et al*. 2021). Fig. 7a shows slight differences in the absorption spectra of pure and Fe/Nd co-doped CoS. These arise due to impurity centres, band gaps, surface roughness and oxygen deficiency. The band gap of CoS pure (3, 5, 7, 9 and 11 at.%) Fe/Nd co-doped CoS nanoparticles, as seen in Fig. 7b, were found to be 3.40eV, 3.50eV, 3.65eV, 3.50eV, 3.81eV and 3.19eV as per the Tauc's plot (energy vs $(\alpha h\nu)^2$. The equation is expressed as

$$(\alpha h\nu)^2 = K(h\nu - Eg)$$

where ν, α, h, Eg and K are the frequency, absorption coefficient, plank constant, band gap and proportionality constant, respectively (Singh *et al*. 2022).

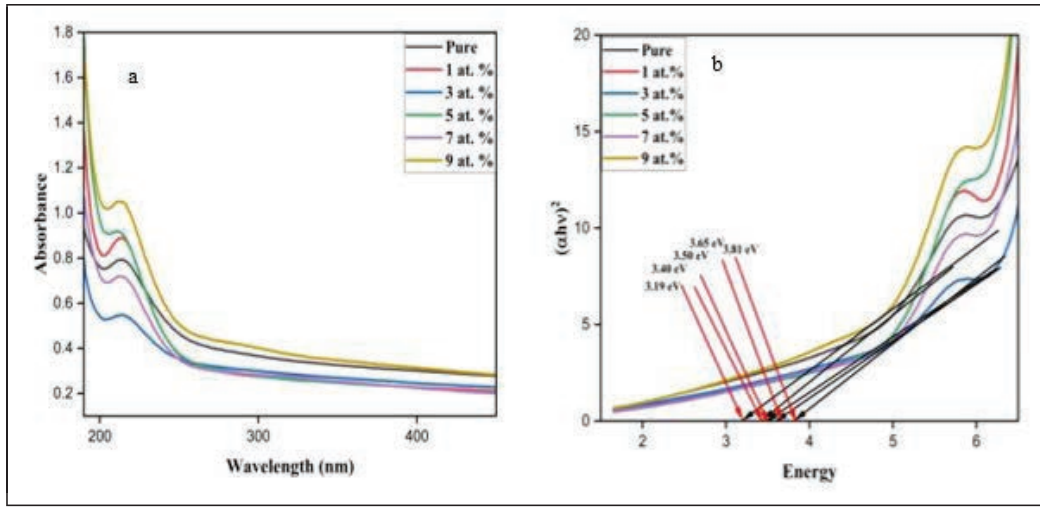

Fig. 7: UV-Visible Spectrum of (a) Pure CoS and Fe/Nd Co-doped CoS at Various Concentrations (b) Tauc Plot for Fe/Nd Co-doped CoS for the Calculation of Band Gap Energy.

Photocatalytic Activity

The degradation of dye methyl red under uv-irradiation every 30, 60, 90, 120, 150, and 180 minutes and in the presence of 7 at.% Fe/Nd co-doped CoS nanoparticles as photocatalyst is shown in Fig. 8a. This research, a novel exploration in the field, unveils the maximum absorption intensity of the dye methyl red at 436 nm, serving as a crucial reference point for studying the degradation abilities of the photocatalyst. The absorption intensity of the dye decreases as the exposure duration increases from 0-180 mins (Singh *et al*. 2020). From the degradation

spectra, we observe a rapid decline in the absorption peak when the catalyst was added to the targeted dye. The enhanced photocatalytic activity of the doping structures, attributed to the ease of electron-hole separation, surface defects, and significant light absorption, is a significant and exciting finding in the field (Cui *et al.* 2015). The doping concentration of 7 at.% might be the optimal value for achieving the best photocatalytic performance. Higher or lower doping concentrations may lead to decreased photocatalytic activity due to changes in the material's electronic structure, defects, or surface properties. Fe and Nd co-doping can introduce electron-hole pairs, enhancing photocatalytic activity. The 7 at.% concentration might balance electron-hole generation & recombination, maximizing the photocatalyst's efficiency.

Furthermore, we study the impact of pH on the degradation percentage of methyl red dye by the above photocatalyst at pH values of 7, 8, 9, and 10. As shown in Fig. 8b, the degradation efficiency is 50%, 60%, 80%, and 70% at pH 7, 8, 9, and 10, respectively. The maximum degradation efficiency is at pH 9 and again decreases at pH 10. The prepared Fe/Nd co-doped CoS under visible light irradiation is photoexcited, leading to the successful degradation of methyl red dye.

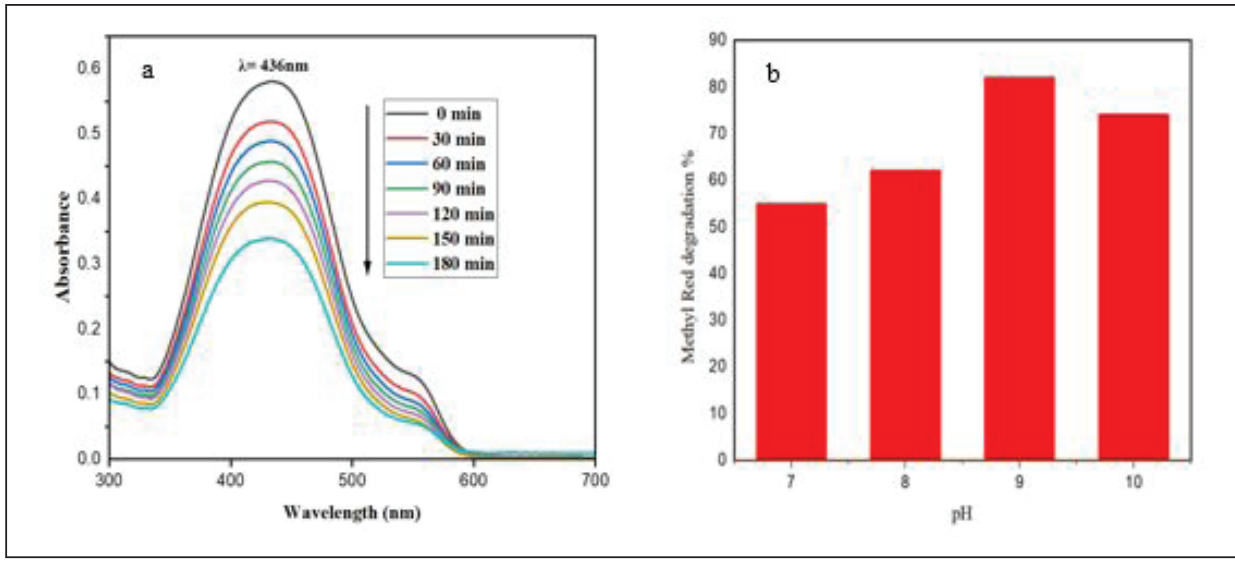

Fig. 8: (a) Time-dependent UV-Vis Absorption Spectra for MR Dye in the Presence of Fe/Nd Co-doped CoS 7 at.%. (b) Degradation Percentage of Methyl Red Dye.

Kinetic Study For Degradation

In general, first-order processes are obeyed by photodegradation of dyes if the plots of $\ln(C_0/C)$ vs time are simple lines (Modrek *et al.* 2013). The pseudo-first-order kinetic of methyl red degradation provided the following description of the photo-catalytic kinetic:

$$v = -dC/dt = -kC \text{ (or } C = C_o e\text{-}k_t) \quad (1)$$

where t is the reaction time, k is the rate constant, C_o is the initial concentration of MR, v is the reaction rate, and C is the MR dye concentration at a specific reaction time. Equation (2) can be used to express the model once equation (1) has been integrated.

$$\ln (C_o/C) = k_t \quad (2)$$

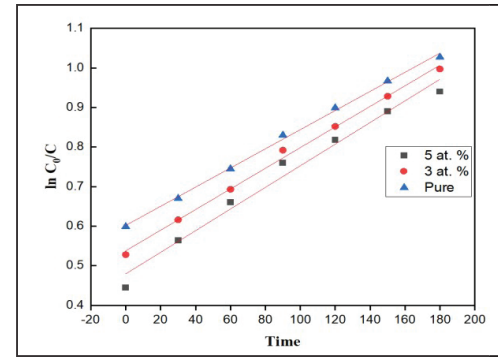

Fig. 9: Plot of Linear Transform ln $[C_o/C]$ vs Irradiation Time in Minutes of the Kinetic Curve of Degradation of Methyl Red Using CoS as Photocatalyst.

A plot of ln (C_o\C) with time will yield a linear plot with slope k (Hein *et al*. 2107). Methylene red dye is discovered to degrade at an observed rate constant of 0.00512 min^{-1} in the presence of a catalyst, and the R^2 values were found to be 0.976, 0.996, and 0.991, respectively.

CONCLUSION

The chemical co-precipitation method was used to synthesize pure and Fe/Nd co-doped CoS nanoparticles, exhibiting a cubic structure in XRD analysis. The functional groups of the pure and doped CoS nanoparticles were visible in their FTIR spectra. Photoluminescence investigations showed an excitation spectrum range of 300-500 nm with strong peaks at 350 and 400 nm and a peak at 470 nm. The emission spectrum ranged from 400-650 nm with 420, 450, and 480 nm peaks. The UV-visible spectrum and the optical band gap of pure and Fe/Nd co-doped CoS nanoparticles from Tauc's plot were found to be in the range of 3.19eV to 3.81eV. Furthermore, the Fe/Nd co-doped CoS catalyst demonstrated higher efficiency in the photodegradation of methyl red dye than the pure sample, making it a promising option for removing organic dye contaminants from wastewater.

ACKNOWLEDGEMENT

The authors express their gratitude to the Department of Chemistry, School of Physical Sciences, DST-Funding, Mizoram University, Aizawl, Mizoram, for providing the cutting-edge instrumentation necessary to meet our specific requirements.

REFERENCES

Li, Y.H.; Tang, Z.R.; Xu, Y.J. Multifunctional graphene-based composite photocatalysts oriented by multifaced roles of graphene in photocatalysis. Chin. J. Catal. 2022;43:708–730.

Jamshaid, M.; Khan, H.M.; Nazir, M.A.; Wattoo, M.A.; Shahzad, K.; Malik, M.; Rehman, A.-U. A novel bentonite–cobalt doped bismuth ferrite nanoparticles with boosted visible light induced photodegradation of methyl orange: Synthesis, characterization and analysis of physiochemical changes. Int. J. Environ. Anal. Chem. 2022.

Rahman, M.Z.; Kibria, M.G.; Mullins, C.B. Metal-free photocatalysts for hydrogen evolution. Chem. Soc. Rev. 2020; 49: 1887–1931.

Mohd Adnan, M.A.; Phoon, B.L.; Muhd Julkapli, N. Mitigation of pollutants by chitosan/metallic oxide photocatalyst: A review. J. Clean. Prod. 2020; 261: 121190.

Wu, X.J.; Xie, S.J.; Zhang, H.K.; Zhang, Q.H.; Sels, B.F.; Wang, Y. Metal Sulfide Photocatalysts for Lignocellulose Valorization. Adv. Mater. 2021; *33*: 2007129

Ma, B.J.; Zhang, R.S.; Lin, K.Y.; Liu, H.X.; Wang, X.Y.; Liu, W.Y.; Zhan, H.J. Large-scale synthesis of noble-metal-free phosphide/CdS composite photocatalysts for enhanced H_2 evolution under visible light irradiation. Chin. J. Catal. 2018; 39: 527–533.

Sobhani, A.; Salavati Niasari, M. Transition metal selenides and diselenides: Hydrothermal fabrication, investigation of morphology, particle size and and their applications in photocatalyst. Adv. Colloid Interface Sci. 2021; 287: 102321.

Li, J.K.; Li, M.; Jin, Z.L. Rational design of a cobalt sulfide/bismuth sulfide S-scheme heterojunction for efficient photocatalytic hydrogen evolution. J. Colloid Interface Sci. 2021; 592: 237–248.

Kokilavani, S.; Syed, A.; Al-Shwaiman, H.A.; Alkhulaifi, M.M.; Almajdhi, F.N.; Elgorban, A.M.; Khan, S.S. Preparation of plasmonic CoS/Ag_2WO_4 nanocomposites: Efficient visible light driven photocatalysts and enhanced anti-microbial activity. Colloid Interface Sci. Commun. 2021; 42: 100415

J. Zhang, Y. Liu, B. Xia, C. Sun, Y. Liu, P. Liu, D. Gao, Facile one-step synthesis of phosphorus-doped CoS_2 as efficient electrocatalyst for hydrogen evolution reaction, Electrochimica Acta .2017; 259: 955-961.

M.B. Muradov, O.O. Balayeva, A.A. Azizov, A.M. Maharramov, L.R. Qahramanli, G.M. Eyvazova, Z.A. Aghamaliyev, Synthesis and characterization of cobalt sulfide nanoparticles by sonochemical method. Infrared Physics & Technology 2018; 89: 255-262.

Zahra Hosseinpour, Zahra Arefinia, Sara Hosseinpour. Cu doped cubic pyrite-type CoS ball like superstructures as heterogeneous photocatalyst. Materials Chemistry and Physics. 2018; 220: 426-432.

N. Mohondas Singh, Monica Lalnunsiami Zadeng, Fidelia Lalrindiki and Lallianmawii. Synthesis, Characterization and Photocatalytic Properties of Pr^{3+} -Doped $CdWO_4$ Using Godzilla Insecticide. Novel Aspects on Chemistry and Biochemistry. 2022; 4: 978-81-19491-04-9.

Singh NP, Singh NR, Singh NM. Synthesis of $CdMoO_4$:Sm^{3+} phosphors at room temperature and investigation on photoluminescence properties. Optik. 2018; 156: 365–373.

G. Gurumoorthy, R. Hema, M. Sundararajan. Synthesis and Characterization of Cobalt Sulfide and Cobalt-Iron Sulfide Nanoparticles from Cobalt (III) Dithiocarbamate Complexes. Annals of the Romanian Society for Cell Biology. 2021; 25(2): 2086–2090.

Naorem RS, Singh NP, Singh NM. Synthesis of SnS_2 photocatalysts and investigation of their photocatalytic activities under sun light irradiation. Advances in Materials and Processing Technologies. 2022; 8(4): 4720- 4730.

Naorem RS, Singh NP, Singh NM. Photoluminescence studies of Ce^{3+} ion-doped $BiPO_4$ phosphor and its photocatalytic activity. International Journal of Applied Ceramic Technology. 2020; 17(6): 2744–2751. DOI: https://doi.org/10.1111/ijac.13600

Chenjuan Zhou, Junjie Luo, Qinqin Chen, Yinzhi Jiang, Xiaoping Dong and Fangming Cui. Titanate nanosheets as highly efficient

non-light-driven catalysts for degradation of organic dyes. Chem. Commun. 2015; 51: 10847-10849.

H. R. Ebrahimi, M. Modrek. Photocatalytic Decomposition of Methyl Red Dye by Using Nanosized Zinc Oxide Deposited on Glass Beads in Various pH and Various Atmosphere. Journal of Chemistry.2013; 2013(5): 151034.

Vo Thi Thu Nhu, Do QuangMinh, Nguyen Ngoc Duy, Nguyen QuocHien .Photocatalytic Degradation of Azo Dye (Methyl Red) In Water under Visible Light Using AgNi/TiO2 Sythesized by γ - Irradiation Method. International Journal of Environment, Agriculture and Biotechnology (IJEAB). 2017; 2(1).